

Holographic Entanglement Entropy in Time Dependent Gauss-Bonnet Gravity

Elena Caceres,^{a,b} Manuel Sanchez^c and Julio Virrueta^{a,d}

^a*Facultad de Ciencias, Universidad de Colima, Bernal Diaz del Castillo 340, Colima, México*

^b*Theory Group, Department of Physics, University of Texas, Austin, TX 78712, USA*

^c*Instituto de Ciencias Nucleares, Universidad Nacional Autónoma de México,
Apartado Postal 70-543, México D.F. 04510, México*

^d*Department of Physics and Astronomy, Stony Brook University, Stony Brook, NY 11794*
E-mail: elenac@zippy.ph.utexas.edu, jmsm.manuel@gmail.com,
juliocesar.morenovirrueta@stonybrook.edu

ABSTRACT: We investigate entanglement entropy in Gauss-Bonnet gravity following a global quench. It is known that in dynamical scenarios the entanglement entropy probe penetrates the apparent horizon. The goal of this work is to study how far behind the horizon can the entanglement probe reach in a Gauss-Bonnet theory. We find that the behavior is quite different depending on the sign of the Gauss-Bonnet coupling λ_{GB} . For $\lambda_{GB} > 0$ the behavior of the probes is just as in Einstein gravity; the probes do not reach the singularity but asymptote to a locus behind the apparent horizon. We calculate the minimum radial position r_{min} reached by the probes and show that for $\lambda_{GB} > 0$ they explore less of the spacetime behind the horizon than in Einstein gravity. On the other hand, for $\lambda_{GB} < 0$ the results are strikingly different; for early times a new family of solutions appears. These new solutions reach arbitrarily close to the singularity. We calculate the entanglement entropy for the two family of solutions with $\lambda_{GB} < 0$ and find that the ones that reach the singularity are the ones of less entanglement entropy. Thus, for $\lambda_{GB} < 0$ the holographic entanglement entropy probes further behind the horizon than in Einstein gravity. In fact, for early times it can explore all the way to the singularity.

Contents

1	Introduction	1
2	Gauss-Bonnet gravity	4
2.1	Time dependent background	5
3	Spacelike geodesics	8
4	Entanglement Entropy	11
4.1	Numerical procedure	13
4.2	Results	14
5	Conclusions and future directions	16
A	Gibbons-Hawking term	20
B	Equations of motion	20
B.1	Minimal volume	20
B.2	Geodesics	21
C	Minimal Volume results	22

1 Introduction

The gauge gravity correspondence postulates the equivalence of a gravity theory and a (non-gravitational) quantum field theory at the boundary. For many years this duality has been successfully applied to translate intractable problems in strongly coupled field theories to manageable calculations in the gravity theory. However, it should be possible to use the correspondence in the reverse direction and learn about quantum gravity. In particular, it should be possible to reconstruct the bulk geometry from CFT boundary data. Much work has been done in this direction in the last few years and many puzzles and surprises have been found along the way. The holographic entanglement entropy prescription (HEE) of Ryu and Takayanagi (RT) [1] has played a crucial role in these discoveries. Unfortunately, our understanding of how local bulk information is encoded in the boundary theory is not yet complete.

Since AdS/CFT geometrizes field theory observables relating them to geometrical constructions one can ask *how much of the spacetime geometry is accessible to the field theory observables?*. This line of work was started in [2],[3] and developed in [4]. In [2] it was shown that spacelike extremal surfaces cannot penetrate the horizon of an asymptotically AdS static black hole but they do penetrate the horizon of a dynamical black hole. It was also noted [2] [3] that even though the probes can explore behind the horizon they do not reach arbitrarily close to the singularity. This behavior was later shown to be related to the linear growth of the entanglement entropy as a function of time [5].

A parallel observation in this line of thought comes from the study of HEE in static AdS black holes with compact boundaries. Typically there are two families of extremal surfaces [3] and we are instructed to choose the one of minimal area as the dual of the entanglement entropy. Which family is the one of minimal area changes depending on where we are in parameter space. The switchover defines a region that the entanglement probe cannot explore and that is dubbed *entanglement shadow* [6] .

Given these limitations of the HEE to access the bulk and thus be used to reconstruct it, it is natural to consider that the HEE might not be the right probe. Indeed, other objects (causal holographic information [7], entwinement [8]) have been proposed either as more natural constructions or as being more suited for bulk reconstruction but it is still not clear what is their field theory dual.

In this work we take a different approach; instead of changing the probe we investigate a different gravity theory. The limitations of the HEE to access the bulk that we mentioned above have been studied in Einstein gravity. Thus, it is natural to ask how are these results modified in a higher derivative theory. Such is the aim of the present work. We study holographic entanglement entropy in a dynamical (Vaydia type) scenario in Gauss-Bonnet gravity where the collapse of a null shell results in the formation of an asymptotically AdS black hole.

Previous studies of HEE in this background have been focused on thermalization time of the field theory. Let us note that in the context of AdS/CFT a Gauss-Bonnet background is dual to a theory with central charges $a \neq c$, and the higher derivative terms arise as corrections in the inverse t'Hooft coupling. The values of λ_{GB} were known to be constraint to a small window by demanding causality of the field theory [9],[10]. These bounds were recently strengthen [11] to show that a consistent holographic theory of quantum gravity with finite λ_{GB} would require an infinite tower of higher spin fields. However, it is still possible to treat the higher derivative terms as part of a perturbative expansion of a string or quantum gravity theory. Thus, such bottom-up approach is used in the thermalization time [12] [13] [14] and anisotropic plasmas in Gauss-Bonnet

[15].

Our interest is not to make contact with a field theory but is more geometric, we want to understand if in higher derivative theories HEE can probe further behind the horizon than in Einstein gravity. In [16] Hubeny, Rangamani and Takayanagi (HRT) presented a covariant generalization of the holographic entanglement entropy prescription of RT. This proposal enabled the holographic study of time dependent phenomena and out of equilibrium physics. The linear growth of entanglement entropy as a function of time typical of ergodic systems was obtained holographically and the thermalization time explored in scenarios with and without chemical potential [17], [18], [19], [20]. The extension of the RT proposal to Gauss-Bonnet theories was initiated in [21] and [22]. In [23], [24] the authors generalized the proposal to arbitrary higher derivatives theories and presented a covariant prescription. Recently, in [25] it was shown that as long as the bulk obeys the null energy condition, the covariant prescription for the entanglement entropy HRT is compatible with causality of the field theory. This point was further explored in higher derivative theories in [26].

In this paper we use these results to study HEE in a Gauss-Bonnet black hole formed by collapsing a null shell. We find that for $\lambda_{GB} > 0$ the HEE surfaces behave just as in Einstein gravity: they penetrate the horizon but stop at a limiting locus and do not reach the singularity. Furthermore, we calculate the minimum point the geodesics can reach behind the horizon and show that for $\lambda_{GB} > 0$ the HEE explores less than HEE in Einstein gravity. For $\lambda_{GB} < 0$ the results are strikingly different: at early times the solutions become double valued with one family reaching the singularity and the other not. Given these two families of solutions the prescription instructs us to choose the one of minimal entropy. We find that it is the family that reaches the singularity the one that has minimal entropy. Thus, our results indicate that for $\lambda_{GB} < 0$ the holographic entanglement entropy can explore all the way to the singularity. For later times the two families join and again HEE no longer explores close to the singularity.

This paper is organized as follows: in Section 2 we summarize some known facts of GB gravity and present the background we will use in the rest of the paper. As a warmup we calculate spacelike geodesics in Section 3 and show that already for spacelike geodesics the curves that reach arbitrarily close to the singularity exist when $\lambda_{GB} < 0$. In Section 4 we present the study of HEE in a Vaidya Gauss-Bonnet background for positive and negative coupling, we explain the numerical procedure and present the results. In the last section (Section 5) we present the conclusions and several possible directions that are, in our opinion, interesting to investigate.

2 Gauss-Bonnet gravity

In the framework of the AdS/CFT correspondence, higher derivatives terms are expected to arise as quantum or stringy corrections to the classical action. Thus, it is compelling to consider an effective action where the cosmological constant and Einstein terms are supplemented by curvature corrections. In this section we will gather some well known facts about one particular such theory: Gauss-Bonnet gravity.

Let us consider five dimensional Gauss-Bonnet gravity. This theory is the simplest of Lovelock theories which are known to yield second order equations of motion in spite containing higher derivative terms in the action. They are free of pathologies and are solvable. In fact, many black hole solutions with AdS asymptotics are known [27].

The action is given by (following the notations in [28], see also [22])

$$S_{grav} = \frac{1}{16\pi G_N} \int d^5x \sqrt{-g} \left(R + \frac{12}{L^2} + \frac{\lambda_{GB} L^2}{2} \mathcal{L}_{(2)} \right), \quad (2.1)$$

$$\mathcal{L}_{(2)} = R_{\mu\nu\rho\sigma} R^{\mu\nu\rho\sigma} - 4R_{\mu\nu} R^{\mu\nu} + R^2 \quad (2.2)$$

Here G_N denotes the five-dimensional Newton's constant, R denotes the Ricci-scalar; the cosmological constant is given by $\Lambda = -12/L^2$, where L is some length scale. Varying the action in (2.1), we get the following equation of motion in (2.1)

$$R_{\mu\nu} - \frac{1}{2}g_{\mu\nu} \left(R + \frac{12}{L^2} + \frac{\lambda_{GB} L^2}{2} \mathcal{L}_{(2)} \right) + \mathcal{H}_{\mu\nu}^{(2)} = 0, \quad (2.3)$$

$$\mathcal{H}_{\mu\nu}^{(2)} = R_{\mu\nu\rho\sigma} \lambda_{GB} R^{\rho\sigma} - 2R_{\mu\rho} R_{\nu}^{\rho} - 2R_{\mu\rho\nu\sigma} R^{\rho\sigma} + R R_{\mu\nu}. \quad (2.4)$$

In some sense, the tensor $\mathcal{H}_{\mu\nu}^{(2)}$ can be thought of as an external energy-momentum tensor sourced by the higher derivative terms.

A solution of the equation of motion (2.3) is¹ [31],

$$ds^2 = -\frac{L^2}{z^2} \frac{f(z)}{f_0} dv^2 + \frac{L^2}{z^2} \left(-\frac{2}{\sqrt{f_0}} dz dv + d\vec{x}^2 \right), \quad (2.5)$$

$$f(z) = \frac{1}{2\lambda_{GB}} [1 - \sqrt{1 - 4\lambda_{GB}(1 - mz^4)}]. \quad (2.6)$$

The background in (2.5) represents an asymptotically AdS-space black hole solution of Gauss-Bonnet gravity where L is related to the radius of curvature and the event-horizon

¹We do not consider the solution with $f(z) = \frac{1}{2\lambda_{GB}} [1 + \sqrt{1 - 4\lambda_{GB}(1 - mz^4)}]$ since it contains ghosts and is unstable [29] [30].

is located at $z_{eh} = m^{-1/4}$. We have expressed the above solution in Eddington-Finkelstein coordinates, which are defined by

$$dt = dv + \sqrt{f_0} \frac{dz}{f(z)} \quad (2.7)$$

where t is the boundary time. Near the boundary, where $z \rightarrow 0$, $v \rightarrow t$. The constant f_0 has been chosen such that $\lim_{z \rightarrow 0} f(z) = f_0$,

$$f_0 = \frac{1}{2\lambda_{GB}} \left(1 - \sqrt{1 - 4\lambda_{GB}} \right). \quad (2.8)$$

we chose to normalize the coordinates in (2.5) such that at the boundary $g_{tt}/g_{xx}|_{z \rightarrow 0} = -1$. In Poincaré patch, the background in (2.5) takes the following form

$$ds^2 = -\frac{L^2}{z^2} \frac{f(z)}{f_0} dt^2 + \frac{L^2}{z^2} d\bar{x}^2 + \frac{L^2}{z^2} \frac{dz^2}{f(z)}. \quad (2.9)$$

Note that the parameter L is related to the AdS curvature scale \tilde{L} as $\tilde{L}^2 = L^2/f_0$. The temperature of this solution is,

$$T = \frac{m^{1/4}}{\pi L^2} \frac{1}{\sqrt{f_0}} \quad (2.10)$$

Note that the event horizon is always located at

$$z_{eh} = m^{-1/4} \quad (2.11)$$

regardless of the value of λ_{GB} . The curvature singularity that occurs at $z = \infty$ for $\lambda_{GB} \geq 0$ is shifted to a finite radial position,

$$z_s = \frac{1}{\sqrt{2}m^{1/4}\lambda_{GB}^{1/4}} (-1 + 4\lambda_{GB})^{1/4} \quad (2.12)$$

for $\lambda_{GB} < 0$.

Finally, throughout this paper we will work with very small values of the Gauss-Bonnet coupling, $\lambda_{GB} = \pm 0.05$ as representatives of positive and negative Gauss-Bonnet couplings.

2.1 Time dependent background

We will now discuss a time-dependent generalization of the background in (2.5). In order to do so, we need to couple the action S_{grav} in (2.1) with an external source term S_{ext} to yield

$$S = S_{grav} + \kappa S_{ext},$$

where κ is some coupling which we do not specify here. A simple solution of the following form can be obtained

$$ds^2 = -\frac{L^2}{z^2} \frac{f(z,v)}{f_0} dv^2 + \frac{L^2}{z^2} \left(-\frac{2}{\sqrt{f_0}} dz dv + d\bar{x}^2 \right), \quad f_0 = \frac{1}{2\lambda_{GB}} (1 - \sqrt{1 - 4\lambda_{GB}}), \quad (2.13)$$

$$f(z,v) = \frac{1}{2\lambda_{GB}} \left[1 - \sqrt{1 - 4\lambda_{GB}(1 - m(v)z^4)} \right]. \quad (2.14)$$

Here $m(v)$ is a function that is hitherto undetermined. It is straightforward to check that the external source must yield the following energy-momentum tensor

$$(16\pi G_N) \kappa T_{\mu\nu}^{ext} = \frac{3}{2} z^3 \frac{dm}{dv} \delta_{\mu\nu} \delta_{vv}. \quad (2.15)$$

Thus a null energy condition on the external energy momentum tensor will give the condition $m'(v) \geq 0$. Null energy condition in the bulk is related to strong subadditivity in the boundary[32],[33]. We want to preserve both of them so we will choose a profile that satisfies $m'(v) \geq 0$ ². Since this is a time-dependent geometry we need to identify the apparent horizon.

A trapped surface T is a co-dimension two spacelike submanifold such that the expansion of both “ingoing” and “outgoing” future directed null geodesics orthogonal to T is everywhere negative. The boundary of the trapped surfaces is the apparent horizon.

In what follows, we will closely follow [34]. For the background in (2.13) the vectors tangent to the ingoing and outgoing null geodesics are given by

$$l_- = -\partial_z, \quad l_+ = -\frac{z^2}{L^2} \partial_v + \frac{z^2}{2L^2} f \sqrt{f_0} \partial_z \quad (2.16)$$

such that

$$l_- \cdot l_- = 0, \quad l_+ \cdot l_+ = 0, \quad l_- \cdot l_+ = -1. \quad (2.17)$$

Now the volume element of the co-dimension two spacelike surface (orthogonal to the above null geodesics) is given by

$$\Sigma = \left(\frac{L}{z} \right)^3. \quad (2.18)$$

The expansions are defined to be

$$\theta_{\pm} = \mathcal{L}_{\pm} \log \Sigma = l_{\pm}^{\mu} \partial_{\mu} (\log \Sigma), \quad (2.19)$$

²This implies that our solutions should produce an $S(\ell)$ that is concave and monotonically increasing [32] and we will see in Section 4.2 that they indeed do.

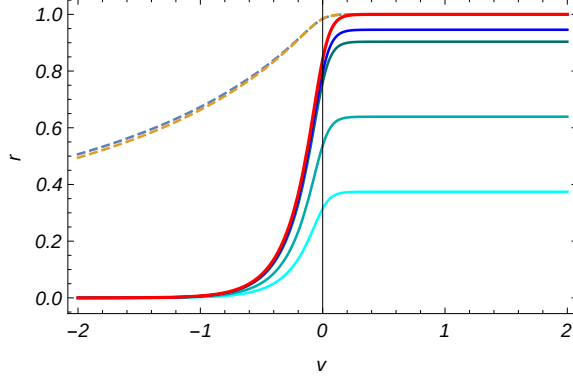


Figure 1. The dashed lines are the event horizons for $\lambda_{GB} = 0.05, -0.05$. The red line is the apparent horizon which is independent of λ_{GB} and the other lines are the singularity for different values of $\lambda_{GB} = -0.005, -0.05, -0.5, -1$, from bottom to top respectively.

where \mathcal{L}_{\pm} denotes the Lie derivatives along the null vectors l_{\pm} . The apparent horizon is then obtained by solving the equation $\Theta = 0$, where $\Theta = \theta_+ \theta_-$ is the invariant quantity. In this case we find

$$\Theta = \frac{9}{2L^2} f(z_{ah}, v) = 0 \quad (2.20)$$

gives the location of the apparent horizon,

$$z_{ah} = m(v)^{-1/4} \quad (2.21)$$

The event horizon, on the other hand, is a null surface in the geometry (2.13),

$$\mathcal{N} = z - z_{eh}(v), \quad G^{\mu\nu} \partial_{\mu} \mathcal{N} \partial_{\nu} \mathcal{N} = 0, \quad (2.22)$$

which gives the evolution of the event horizon,

$$z'_{eh}(v) = -\frac{1}{2\sqrt{f_0}} f(z_{eh}, v). \quad (2.23)$$

It is clear from (2.20) that the position of the apparent horizon does not depend on λ_{GB} . However, the position of the event horizon does albeit mildly (see Figure 1)

Our goal in the next sections is to study non-local probes in (2.13) that evolves between a vacuum AdS geometry with radius and an asymptotically AdS black hole solution of Gauss Bonnet action (2.1). We will be particularly interested in comparing how far behind the apparent horizon the different probes can reach. Our main interest is the behavior of the entanglement entropy, Section 4. However, we will first analyze spacelike geodesics which already illustrate some novel features also present in the entanglement entropy.

3 Spacelike geodesics

To find spacelike geodesics in the background (2.13) we extremize the following Lagrangian

$$\mathcal{L} = \frac{1}{z(x)} \sqrt{f_0 - f(z, v)v'(x)^2 - 2\sqrt{f_0}v'(x)z'(x)} \quad (3.1)$$

The equations of motion are³

$$\begin{aligned} z''(x) &= \mathcal{Z}[v(x), z(x)] \\ v''(x) &= \mathcal{V}[v(x), z(x)] \end{aligned} \quad (3.2)$$

The equations of motion will be solved subject to boundary conditions

$$z(l/2) = z(-l/2) = z_0 \quad \text{and} \quad z'(0) = v'(0) = 0$$

where $l/2$ denotes the distance in the boundary and z_0 is the IR cutoff. The Lagrangian (3.1) does not depend explicitly on x , the corresponding conserved quantity is,

$$\frac{1}{z(x)^2 \mathcal{L}} = C_1. \quad (3.3)$$

We will be working with a thin shell, $M(v) = \frac{1}{2}(1 + \tanh(v/v_0))$ with $v_0 = 0.01$. As the parameter v_0 goes to zero, this function approximates a step function. Thus, in the limit $v_0 \rightarrow 0$ the spacetime is given by the gluing of two static geometries. Let us pause and, to gain some intuition, briefly study the behavior of geodesics in static Gauss Bonnet spaces.

If $M(v) = m$, v is a cyclic variable and its associated momentum is conserved,

$$\frac{-f(z)v'(x) - \sqrt{f_0}z'(x)}{z(x)^2 \mathcal{L}} = C_2 \quad (3.4)$$

Thus, in the static case we have two conserved quantities (3.3) and (3.4). It is instructive to find the effective potential in this case since it will illustrate the differences for $\lambda_{GB} > 0$ and $\lambda_{GB} < 0$ that will persist in the dynamic case. Solving (3.3) for $v'(x)$ and substituting in (3.4) we get

$$z'(x)^2 = E^2 - V_{eff} \quad (3.5)$$

where

$$V_{eff} = f(z, \lambda_{GB}) \left(1 - \frac{\mathcal{J}^2}{z^2}\right). \quad (3.6)$$

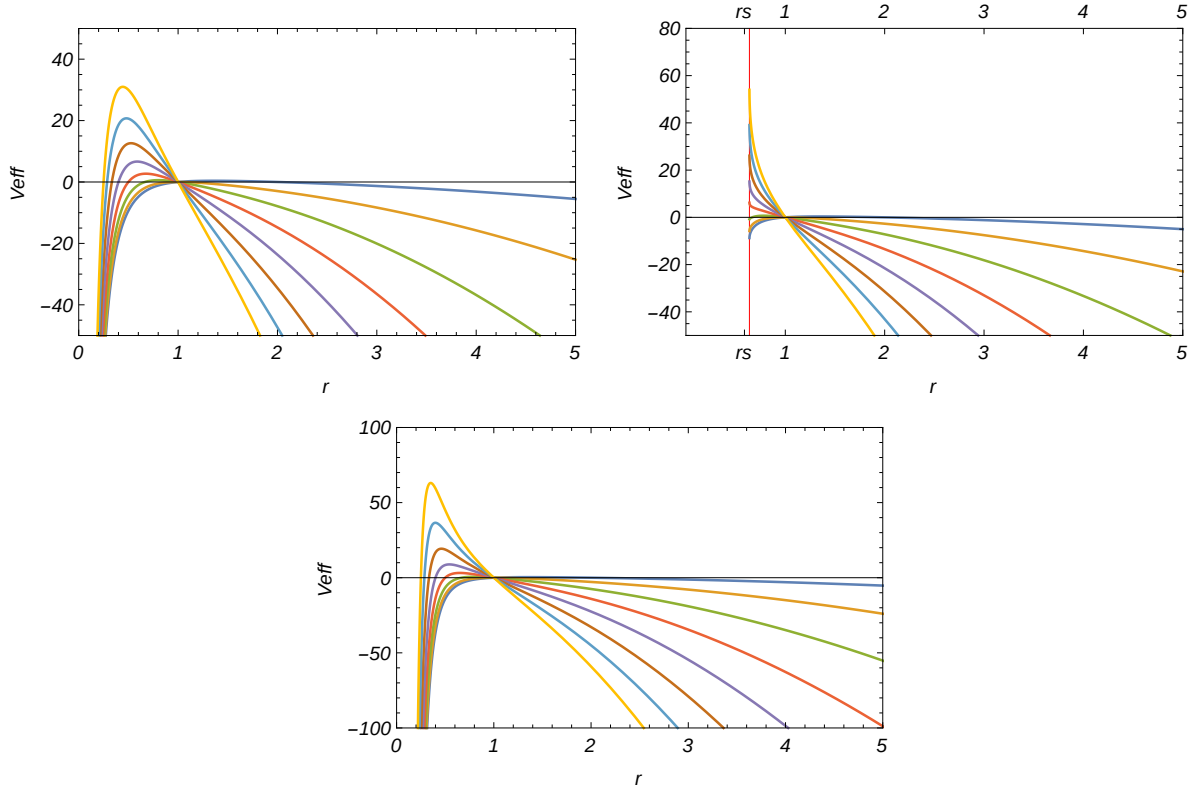


Figure 2. Effective potential $V_{eff}(r)$ for $m = 1$ and different values of \mathcal{J} . Left panel : $\lambda_{GB} = .05$. Right panel: $\lambda_{GB} = -0.05$. In the lower panel we have included the *SAdS* case for comparison.

For convenience we have redefined the constants as $E = \frac{C_2}{C_1} \sqrt{f_0(\lambda_{GB})}$ and $\mathcal{J} = \frac{1}{C_1}$. In Figure (2) we plot V_{eff} for different values of C_1 as a function of $r = 1/z$. Note the different behavior of the potential for $\lambda_{GB} > 0$ and $\lambda_{GB} < 0$. For $\lambda_{GB} > 0$ the potential is similar to the Schwarzschild *AdS*₅ (*SAdS*₅); it reaches a maximum for some value of $0 < r < r_h$ and the value of the maximum grows with large \mathcal{J} . The growth of this maximum becomes less pronounced as we increase λ_{GB} . For $\lambda_{GB} < 0$ the potential is qualitatively different. For small values of \mathcal{J} it is a concave function that reaches its maximum at some $r_s < r < r_h$ similar to the positive λ_{GB} case. However, for large \mathcal{J} the concavity of the potential changes and reaches its maximum at the singularity r_s . We identify the critical value of \mathcal{J} at which this change occurs,

$$\mathcal{J}_{crit} \sim \frac{1}{2\sqrt{-\lambda_{GB}}(1 + 2\lambda_{GB})}. \quad (3.7)$$

³The explicit form of the functionals $\mathcal{Z}[v(x), z(x)]$ and $\mathcal{V}[v(x), z(x)]$ are given in Appendix B

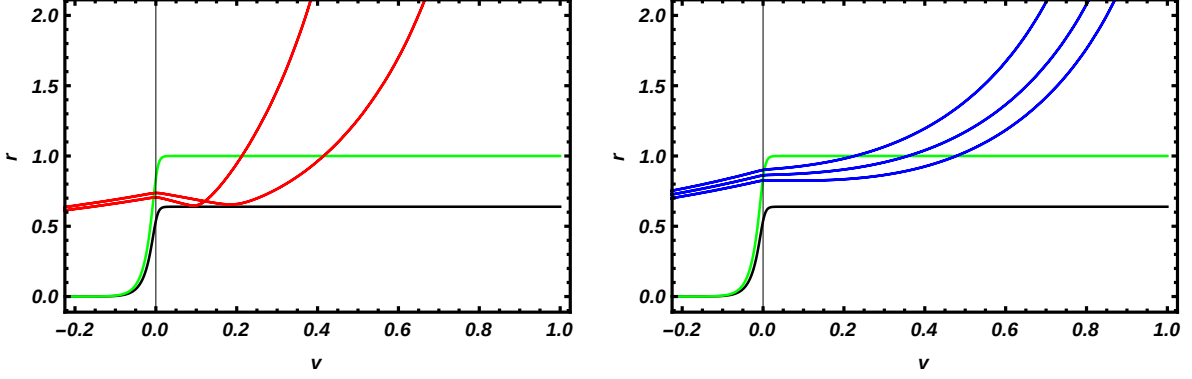


Figure 3. Representative geodesics for negative λ_{GB} . Left panel: the new family of solutions that reach the singularity. Right panel: the standard solutions that asymptote to a critical surface and do not reach the singularity.

The existence of this different regimes in the case of negative λ_{GB} is clearly associated with the fact that the singularity has shifted from $r = 0$ to $r_s^{-1} = \frac{1}{\sqrt{2}m^{1/4}\lambda_{GB}^{1/4}}(-1 + 4\lambda_{GB})^{1/4}$. This different behavior of V_{eff} for $\lambda_{GB} < 0$ and $\lambda_{GB} > 0$ will be reflected in the time dependent case.

Now we are ready to proceed with the time dependent case with $M(v)$ in (2.13) given by $M(v) = \frac{1}{2}(1 + \tanh \frac{v}{v_0})$. We want to solve the differential equations 3.2 subject to the following boundary conditions

$$z(0) = z_*, \quad z'(0) = 0, \quad v(0) = v_*, \quad v'(0) = 0$$

So far z_* and v_* are two free parameters that generate the numerical solutions for $z(x)$ and $v(x)$. Once a solution is obtained the boundary data can be read off,

$$z(l/2) = z_0 \quad v(l/2) = t_b$$

. Note that the numerically nontrivial part is to look for appropriate parameters (z_*, v_*) such that the IR cutoff z_0 is a small number ⁴. We will expand on the details of the numerical procedure in section (4.1) when we deal with the HEE probes that is our main objective.

We solve the equations of motion and look for geodesics that cross the horizon and are anchored at the boundary. We find that the case of negative λ_{GB} presents some new features. There are geodesics that, as in SAdS-Vaidya, cross the horizon but do not reach the singularity and asymptote to a limiting surface. But there is also – for some range of parameters– a new family of boundary anchored geodesics that do reach arbitrarily close to the singularity. It is remarkable that this strikingly different behavior

⁴In our solutions we demand $z_0 \sim 10^{-5}$

depends crucially on the sign of λ_{GB} and is present even for such a small value of the coupling as $\lambda_{GB} = -0.05$. In Figure (3) we plot some representative solutions.

4 Entanglement Entropy

The proposal for computing entanglement entropy is modified according to the formula obtained in [22] [21]

$$S_{EE} = \frac{1}{4G_N} \int_{\Sigma} d^3\xi \sqrt{\gamma} (1 + \lambda_{GB} L^2 R_{\Sigma}) + \frac{1}{2G_N} \int_{\partial\Sigma} d^2\xi \sqrt{h} K, \quad (4.1)$$

where Σ denotes the three dimensional surface anchored at the two dimensional boundary of the region A; ξ denotes the worldvolume coordinates on the surface and h denotes the induced metric on this surface. The quantity R_{Σ} denotes the Ricci scalar constructed from the induced metric on Σ and the last term in (4.1) is the Gibbons-Hawking boundary term that one needs to introduce to have well a defined variational problem. The proposal (4.1) was initially put forward for time independent situations. In [23],[24] the authors generalize the proposal of [22], [21] and presented a covariant prescription valid for more general theories of higher derivatives.

Throughout this paper we will study the “rectangular strip” in the backgrounds (2.13). Assuming translational invariance in two of the directions we can parametrize the extremal area surface by the third coordinate, x , and we have $z(x), v(x)$. We denote the width of the rectangular strip ℓ , that is $\frac{\ell}{2} < x < \frac{\ell}{2}$. The induced metric on the co-dimension two surface is given by

$$ds^2 = \frac{L^2}{z^2} (dx_2^2 + dx_3^2) + \frac{L^2}{z^2} \left(1 - \frac{f}{f_0} v'^2 - \frac{2}{\sqrt{f_0}} v' z' \right) dx^2, \quad (4.2)$$

where once more we have $' \equiv d/dx$. This now gives

$$\sqrt{\gamma} = \frac{L^3}{\sqrt{f_0}} \frac{1}{z^3} \left(f_0 - f v'^2 - 2\sqrt{f_0} v' z' \right)^{1/2}, \quad (4.3)$$

$$\lambda_{GB} L^2 \sqrt{\gamma} R_{\Sigma} = (2L^3 \lambda_{GB} \sqrt{f_0}) \frac{z'^2}{z^3 (f_0 - f v'^2 - 2\sqrt{f_0} v' z')^{1/2}} + \frac{dF}{dz}, \quad (4.4)$$

where

$$F(x) = (4L^3 \lambda_{GB} \sqrt{f_0}) \frac{z'}{z^2 (f_0 - f v'^2 - 2\sqrt{f_0} v' z')^{1/2}} \quad (4.5)$$

Clearly, the total derivative term will not contribute to the equations of motion. Furthermore, the dF/dx term is exactly cancelled by the Gibbons-Hawking term⁵. Thus, the effective action that needs to be extremized is given

$$S_{eff} = \frac{L^3}{4G_N\sqrt{f_0}} \int \frac{dz}{z^3} \left[\left(f_0 - f v'^2 - 2\sqrt{f_0} v' z' \right)^{1/2} + \frac{2\lambda_{GB} f_0 z'^2}{\left(f_0 - f v'^2 - 2\sqrt{f_0} v' z' \right)^{1/2}} \right]. \quad (4.6)$$

The equations of motion derived from (4.6) are,

$$z'' = \frac{F_z(z, z', v, v')}{G(z, z', v, v')} \quad (4.7)$$

$$v'' = \frac{F_v(z, z', v, v')}{G(z, z', v, v')} \quad (4.8)$$

where we are not writing explicitly the x dependence in $z(x)$, $v(x)$ and $'$ denotes derivative with respect to x .

$$\begin{aligned} F_z = & \sqrt{f_0} f(z, v) \left[\sqrt{f_0} v'^2 \left[(6\lambda_{GB} z z'^2 - z) \partial_z f(z, v) - 24 z'^2 \right] \right. \\ & + 4 z v'^3 z' \partial_z f(z, v) + z v'^4 \partial_v f(z, v) + 6 f_0^{3/2} (2\lambda_{GB} z'^2 - 1) - 24 f_0 v' z' (\lambda_{GB} z'^2 - 1) \left. \right] \\ & + v'^2 f(z, v)^2 \left[z v'^2 f^{(1,0)}(z, v) - 24 \sqrt{f_0} v' z' - 12 f_0 (\lambda_{GB} z'^2 - 1) \right] \\ & + f_0 z v' \left[v' \partial_v f(z, v) + 2 z' \partial_z f(z, v) \right] \left[6 \lambda_{GB} \sqrt{f_0} z'^2 - \sqrt{f_0} + 2 v' z' \right] - 6 v'^4 f(z, v)^3 \end{aligned} \quad (4.9)$$

$$\begin{aligned} F_v = & z v' \partial_z f(z, v) \left[-2 \sqrt{f_0} z' \left[v'^2 - 4 \lambda_{GB} v'^2 f(z, v) + 4 f_0 \lambda_{GB} \right] \right. \\ & + v' \left[f_0 - v'^2 f(z, v) \right] + 10 f_0 \lambda_{GB} v' z'^2 \left. \right] - 2 \left[f_0 - v' \left(v' f(z, v) + 2 \sqrt{f_0} z' \right) \right] \\ & \times \left[2 \sqrt{f_0} \left(\lambda_{GB} z v'^2 \partial_v f(z, v) + 3 z' \left(\sqrt{f_0} \lambda_{GB} z' + v' \right) \right) + 3 v'^2 f(z, v) - 3 f_0 \right] \end{aligned} \quad (4.10)$$

$$G = 2 \sqrt{f_0} z \left[(4 \lambda_{GB} f(z, v) + 1) \left(v'^2 (-f(z, v)) - 2 \sqrt{f_0} v' z' + f_0 \right) - 6 f_0 \lambda_{GB} z'^2 \right] \quad (4.11)$$

⁵Note that in [23],[24] the prescription does not include a boundary term and dF/dx is not cancelled. It is clear that the solutions of the extremization procedure will be the same whether dF/dx is present or not. However, the value of the entanglement entropy might change. In the present case one can check that the contribution of dF/dx is divergent and thus will be subtracted after normalization. We thank Tomás Andrade for comments on this issue

We will solve these equations of motion subject to the initial conditions,

$$z(0) = z_*, \quad z'(0) = 0 \quad (4.12)$$

and,

$$v(0) = v_*, \quad v'(0) = 0. \quad (4.13)$$

Thus a particular solution is labeled by (z_*, v_*) . We are interested in (z_*, v_*) that produce surfaces anchored at the boundary. We also want relate these constants to boundary quantities ℓ and t_b . The numerical procedure used to do this is explained below.

4.1 Numerical procedure

In order to solve the motion equation numerically, we employ the Dormand-Prince method [35], which is an explicit method to solve systems of differential equations. This method uses six evaluations to compute the fourth and fifth order solutions and employ them to estimate the relative error, once determined the error, the program uses an automatic step adjusting procedure. In the present work we used the C language implementation of the Dormand-Prince method provided by [36]. Notice that the condition that the homology condition, in this case equivalent to demanding that the surface is anchored at the boundary, is not included a priori on the system of differential equations, they need to be considered during the selection of initial conditions. Because the solutions diverges at the boundary, it is not possible to set the initial conditions there. However, since we know that at least in two points $z \rightarrow 0$, there is a maximum point z_* , by translational invariance we may set

$$z(0) = z_*, \quad z'(0) = 0 \quad (4.14)$$

this completely fixes the initial conditions for $z(x)$. In a similar way we impose the initial conditions for $v(x)$ to be

$$v(0) = v_*, \quad v'(0) = 0. \quad (4.15)$$

Then we may parametrize the set of all the solutions by (z_*, v_*) . We want to relate the parameters (z_*, v_*) with the parameters at the boundary (ℓ, t_b) , to do so we notice that, by symmetry, $z(\pm\ell/2) = 0$ and $v(\pm\ell/2) = t_b$. These equations establish a relation between the two set of parameters, however it is not possible to solve them in general. Instead of that we proceed to scan the parameter space (z_*, v_*) in the region $z_* \in (0, 10]$ and $v_* \in [-10, 10]$ using a grid of 600×600 or 800×800 over applied over different subregions. The grid size and the region to be explored were chosen to maximize the number of curves satisfying the homology condition and crossing the apparent horizon. In order

to solve the system of differential equation over the grid in a more efficient way we divide the process into 10 or 20 parallel processors. Once obtained a list of acceptable initial conditions, those which are anchored at the boundary, we proceed to choose those solutions which satisfied any required boundary conditions, i.e. ℓ and t_b , the precision with which those values are determined depends on the grid step, for the present work we keep a precision in the boundary condition determination of ± 0.05 . After solving the system of equations and properly imposing the homology condition we now need to evaluate the entanglement entropy function on-shell, this procedure needs to be done numerically as well.

We need to be careful due the divergent behaviour of the integral at the boundary. For the static cases this is solved by using the conserved quantity to write the integral in terms of z , imposing a UV cut-off z_0 and subtracting the divergent contribution. In static Gauss-Bonnet backgrounds the divergent contribution can be computed in a standard way in the static limit by subtracting the vacuum contribution. However, it will depend on λ_{GB} . This stems from the fact that vacuum Gauss-Bonnet is an AdS space but with a λ_{GB} dependent radius.

In the dynamic case that procedure cannot be employed since we have no conserved quantities, although the divergent contribution to the integral is the same as in the static case, the problem arises when determining the proper way to impose a UV cut-off in a consistent way, this is which match with the static cut-off in the asymptotic limit. Instead of directly impose a cut in the x interval, we employ the numerical integration algorithm itself, imposing a desire precision and a maximal number of step reduction, once reached those values the integral is declared as divergent and the integration finished at that value of x .

4.2 Results

We carried out a numerical study of HEE in backgrounds with $\lambda_{GB} = 0.05$ and $\lambda_{GB} = -.05$ as representatives of theories with positive and negative λ_{GB} . We find that while for positive λ_{GB} the behavior of the extremal surface solution of (4.7) is qualitatively similar to the case of Einstein gravity, for negative λ_{GB} it is strikingly different. We summarize our results below:

- For $\lambda_{GB} < 0$ and for early times and $\ell \geq 2.5$ a new family of solution appears. That is, for a given t_b and ℓ two solutions are possible: one that behaves just like $\lambda_{GB} > 0$, we denote this family \mathcal{M}^0 , and one that probes arbitrarily close to the singularity, \mathcal{M}^S , Fig.(4).

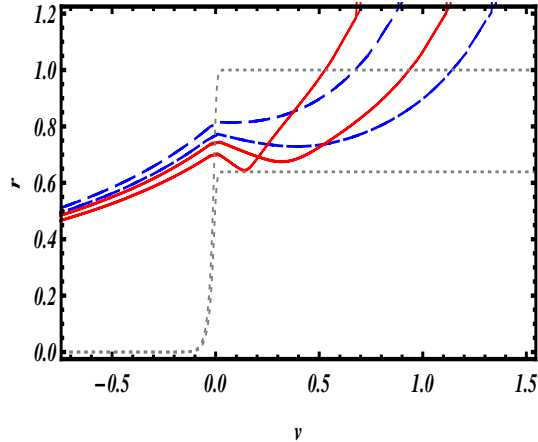


Figure 4. Representatives of the two families of minimal surfaces for negative Gauss Bonnet coupling, $\lambda_{GB} = -0.05$. The family \mathcal{M}^S , red curves, contains surfaces that probe arbitrarily close to the singularity. The family \mathcal{M}^0 , dashed curves, is very similar to the $SAdS$ and $\lambda_{GB} > 0$, they explore behind the horizon but do not reach the singularity.

- We studied the minima, r_{min} , reached by the extremal surfaces and present the results in Fig. (5). We can see that for early times the family \mathcal{M}^S probes arbitrarily close to the singularity $r_{min}^S \sim r_s$, where r_s^{-1} is defined in (2.12). As time increases r_{min}^S becomes larger and for later times the minima converge such that $r_{min}^S \sim r_{min}^0 \sim r_{min}^{\lambda_{GB}>0} \sim r_{min}^{SAdS}$.
- We evaluate the functional in these solutions and find that the one that penetrates deeper behind the horizon, close to the singularity, is the one that represents the entanglement entropy Fig.(6).
- As a check of our solutions we calculated entanglement entropy as a function of ℓ . The concavity of this curve is associated with the validity of strong subadditivity [32], [37]. We find that our solutions obey SSA as expected.
- The $\lambda_{GB} > 0$ case is very similar to $SAdS$, the extremal surfaces penetrate the horizon but only up to a limiting surface. When we compare the minima we find that for $\lambda_{GB} > 0$ the extremal surfaces explore less than in the AdS geometry Fig.(5).
- As mention in section (4) the prescription of for the entanglement entropy in a Gauss Bonnet theory is not just a minimal volume as in Einstein gravity. It is natural to ask if the new effects seen here for $\lambda_{GB} < 0$ are due to the extra term in the functional or if they are already present in a minimal volume. In order

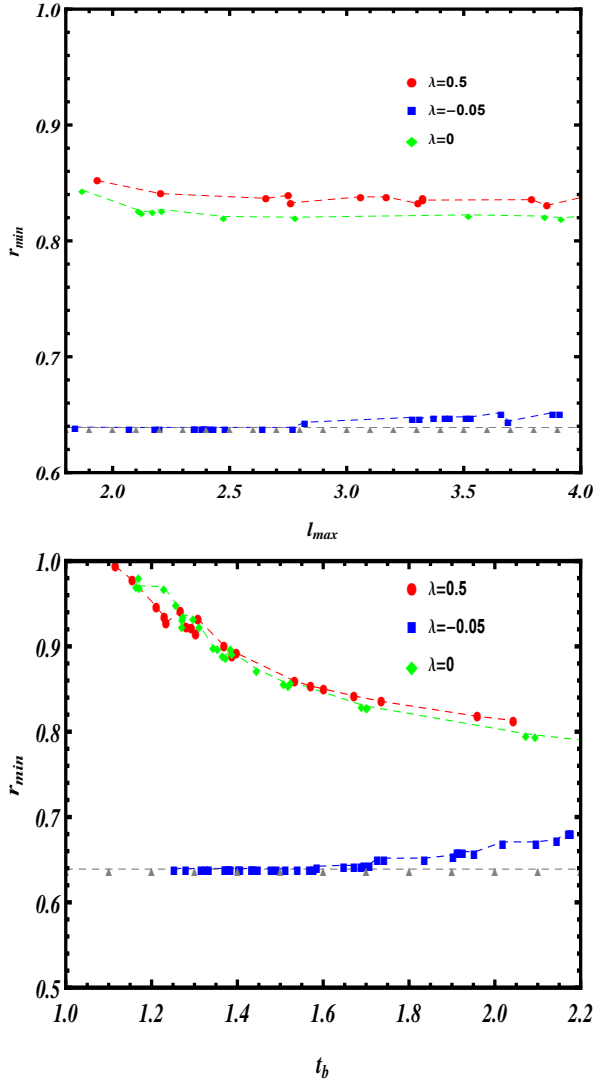


Figure 5. The minimum point reached by a given entanglement entropy surface for $SAdS$, green, $\lambda_{GB} > 0$, red, and $\lambda_{GB} < 0$, blue. Top panel: r_{min} as function of the boundary separation ℓ . Bottom panel: r_{min} as function of the boundary time t_b .

to elucidate this point we calculate the minimal volume for strip regions in an asymptotically AdS Gauss Bonnet black hole (2.13). We find that the minimal volumes also reach close to the singularity in the case of $\lambda_{GB} < 0$. We present the corresponding figures in Appendix (C).

5 Conclusions and future directions

The main motivation of this work is a simple question, *how far behind the horizon does the HEE probe reach in Gauss-Bonnet theories?*. Much is known about the similar question

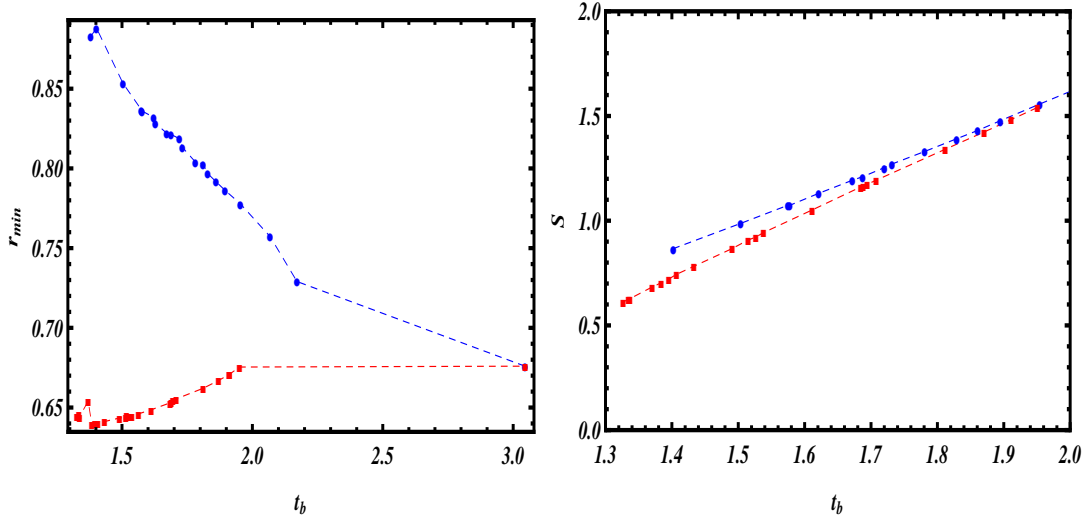


Figure 6. Left panel: minima for the two families of extremal surfaces \mathcal{M}^S , red and \mathcal{M}^0 , blue. Right panel: Their corresponding entanglement entropy .

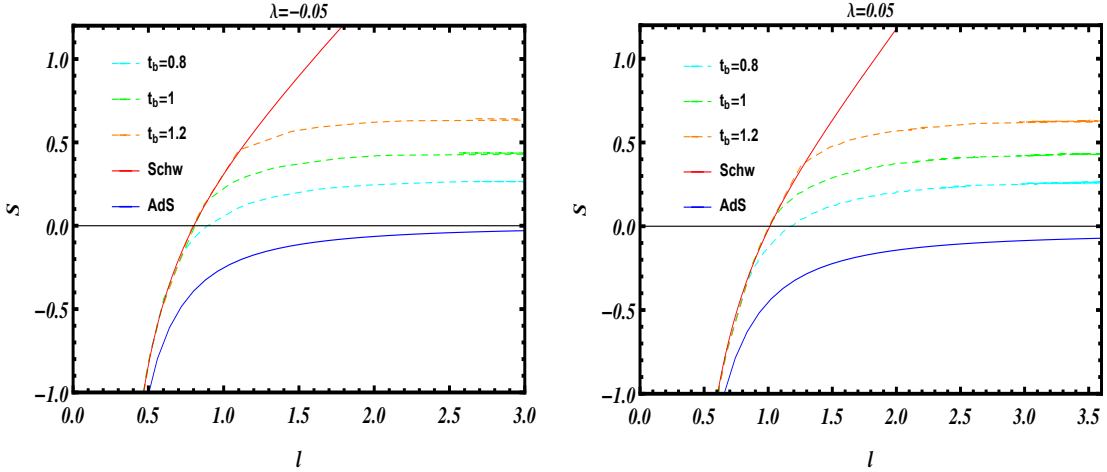


Figure 7. Entanglement entropy as a function of ℓ for $\lambda_{GB} = -.05$ (left panel) and $\lambda_{GB} = .05$ (right panel)

in Einstein gravity but previous studies in Gauss-Bonnet have focused in finding the thermalization time and not in the reach of the probes. In the AdS/CFT context higher derivative theories are interesting because they are dual to field theories with corrections in $1/\sqrt{g_{YM}N}$. We chose Gauss-Bonnet as example of a higher derivative theory because of its solvability; there are black hole solutions known analytically. We take Gauss-Bonnet as a toy model where to learn features of holographic entanglement entropy in a higher derivative theory and not as a dual of a particular field theory. As a warmup we studied geodesics in a Vaidya Gauss-Bonnet background. When λ_{GB} is positive there

are no surprises, the holographic probes behaves as in Einstein gravity. Namely, they penetrate behind the apparent horizon but not arbitrarily close to the singularity; they asymptote to a certain critical surface. A different and novel behavior appears when we consider $\lambda_{GB} < 0$: the solutions become double valued. A new family of solutions that can reach arbitrarily close to the singularity appears. We observe the same behavior in minimal volume surfaces. However, in a 5 dimensional bulk these objects are purely geometric, they are not dual to any field theory observable.

Unlike in Einstein gravity, the holographic entanglement entropy prescription for higher derivative theories [24],[23] is not only a minimal area but includes an extra term involving the extrinsic curvature. We study the entanglement entropy in a Vaidya Gauss-Bonnet background and quantify how much behind the horizon the probes reach, r_{min} , and find that for $\lambda_{GB} > 0$ the probes explore less than in Einstein gravity, *i.e.* $r_{min}^{GB} > r_{min}^{Einstein}$.

For $\lambda_{GB} < 0$ we find two family of solutions: one that behaves very similar to Einstein gravity and a new one that reaches arbitrarily close to the singularity. Having two solutions the HRT prescription instruct us to choose the one of minimal entropy. We find that the surfaces reaching the singularity are the ones of minimal entropy. Thus, *for $\lambda_{GB} < 0$ the holographic entanglement entropy can probe all the way to the singularity.* This is the main result of the present work. As a check of our solutions we verify the concavity of $S(l)$ implying that SSA is respected.

Let us point some open problems and future directions related to the present work;

- *Lionhearted effort:* Because of its time dependent nature, the problem studied here is numerically intensive. We have concentrated in $\lambda_{GB} = 0.05$ and $\lambda_{GB} = -0.05$ as representatives of positive and negative couplings. A complete analysis scanning over a range of values of λ_{GB} would certainly be desirable and interesting and might uncover interesting physics as λ_{GB} becomes larger. In particular, the novel solutions discovered here for negative λ_{GB} (the ones that can reach the singularity) exist only for a very short time after the probe has crossed the shell. It is natural to think that as λ_{GB} grows more negative these type of solutions will exist for a larger time. Or it could be that the opposite is true, that for larger negative λ_{GB} these solutions cease to exist. The only way to answer these questions is a full numerical analysis over the λ_{GB} parameter space.
- An immediate generalization of the present work would be to study spacetimes of dimensions higher than 5 and boundary regions other than the strip.
- It would be interesting to ask the same question investigated here in other higher derivative theories like more general Lovelock theories where many black hole so-

lutions are known [27]. Also, thermalization in hyperscaling violating backgrounds was investigated in [38],[39] and higher derivative corrections in [40],[41]. Thus, extending the present work to hyperscaling violating geometries seems a viable and interesting endeavor.

- We have studied entanglement entropy in a time dependent Gauss-Bonnet background in Poincare patch. In the static case, it is known that novel features of the entanglement entropy appear when considering compact spaces [3]. Thus, extending the present work to spherically symmetric spaces might also uncover some new phenomena sensitive to the sign of the Gauss-Bonnet coupling λ_{GB} .
- In the same spirit of understanding how much of the bulk does the HEE probes, it would be interesting to consider an asymptotically global AdS static black hole in Gauss-Bonnet gravity and study the entanglement shadow. We expect that entanglement shadow will increase or decrease (as compared to Einstein gravity) depending on the sign of λ_{GB} .
- It would be interesting to perform a similar study with different holographic probes like the causal holographic information. The acausality of the boundary theory for finite λ_{GB} might be reflected in some particular behavior of the causal holographic information surface χ_A .
- In [42] a formalism was developed to study black hole formation in a weak field limit. As shown in [43] some of the interesting physics discovered using the Vaidya model for charged black holes [18] can be captured in the weak field approach. Although valid only after a certain time after collapse, the advantage of the perturbative approach is that it is numerically simpler. Thus, it would be interesting to investigate scalar collapse in a Gauss Bonnet theory in the weak field limit and see if some of the results presented here can be also obtained in that framework.

We hope to return to some of these problems in the near future.

Acknowledgments

It is a pleasure to thank Tomás Andrade, Veronika Hubeny, Cindy Keeler, Yi Pang and Juan Pedraza for useful discussions. This research was supported by Mexico's National Council of Science and Technology (CONACyT) grant CB-2014-01-238734 and the National Science Foundation under Grant PHY-1316033 and Grant No. NSF PHY11-25915. E.C thanks the Galileo Galilei Institute for Theoretical Physics and the Kavli

Institute for Theoretical Physics for hospitality and the INFN for partial support during the completion of this work.

A Gibbons-Hawking term

In this appendix we provide details of the calculation of the boundary term,

$$S_{GH} = \oint_{\partial\Sigma} \sqrt{h} \mathcal{K}.$$

To fix notation, recall that the integral [A](#) is over the boundary of the codimension 2 surface Σ with induced metric γ , h is the metric induced at the boundary and \mathcal{K} the trace of the extrinsic curvature of Σ .

As we saw in [4.2](#), the metric induced in the co-dimension two surface is

$$\gamma_{ab} dx^a dx^b = \frac{L^2}{z^2} \left(1 - \frac{f}{f_0} v'^2 - \frac{2}{\sqrt{f_0}} v' z' \right) dx^2 + \frac{L^2}{z^2} (dx_2^2 + dx_3^2), \quad (1.1)$$

The unit norm vector perpendicular to the boundary is clearly in the x direction,

$$\eta = \left(\frac{L}{z} \sqrt{\left(1 - \frac{f}{f_0} v'^2 - \frac{2}{\sqrt{f_0}} v' z' \right)}, 0, 0 \right)$$

the trace of the extrinsic curvature is then

$$\mathcal{K} = \gamma^{ab} \nabla_a \eta_b = 2 \frac{z' \sqrt{f_0}}{L \sqrt{f_0 + f v'^2 - 2 \sqrt{f_0} v' z'}}$$

Now, the determinant of the metric induced at the boundary is simply $\frac{L^2}{z^2}$. Thus we have

$$S_{GH} = \oint_{\partial\gamma} dx_2 dx_3 2L \frac{z' \sqrt{f_0}}{z^2 \sqrt{f_0 + f v'^2 - 2 \sqrt{f_0} v' z'}}$$

which exactly cancels the term $\int \frac{dF}{dx}$ in [4.4](#).

B Equations of motion

B.1 Minimal volume

$$\mathcal{L} = \frac{1}{z^3} \sqrt{f_0 - f(z, v) v'^2 - 2 \sqrt{f_0} v' z'} \quad (2.1)$$

The equations of motion are,

$$z'' = \frac{F_z(z, z', v, v')}{G(z, z', v, v')} \quad (2.2)$$

$$v'' = \frac{F_v(z, z', v, v')}{G(z, z', v, v')} \quad (2.3)$$

where we are not writing explicitly the x dependence in $z(x)$, $v(x)$ and $'$ denotes derivative with respect to x .

$$F_z = -(6f(z, v)^2 v'^2 + f(z, v)(6f_0 + 12\sqrt{f_0}v'z' + zv'^2\partial_z f(z, v))\sqrt{f_0}zv'(v'\partial_v f(z, v) + 2z'\partial_z f(z, v))) \quad (2.4)$$

$$F_v = 6f_0 - 12\sqrt{f_0}v'z' + v'^2(-6f(z, v) + z\partial_z f(z, v)) \quad (2.5)$$

$$G = 2\sqrt{f_0}z \quad (2.6)$$

B.2 Geodesics

$$\mathcal{L} = \frac{1}{z}\sqrt{f_0 - f(z, v)v'^2 - 2\sqrt{f_0}v'z'} \quad (2.7)$$

The equations of motion are,

$$z'' = \frac{F_z(z, z', v, v')}{G(z, z', v, v')} \quad (2.8)$$

$$v'' = \frac{F_v(z, z', v, v')}{G(z, z', v, v')} \quad (2.9)$$

$$F_z = -(2f(z, v)^2 v'^2 + f(z, v)(2f_0 + 4\sqrt{f_0}v'z' + zv'^2\partial_z f(z, v))\sqrt{f_0}zv'(v'\partial_v f(z, v) + 2z'\partial_z f(z, v))) \quad (2.10)$$

$$F_v = 2f_0 - 4\sqrt{f_0}v'z' + v'^2(-2f(z, v) + z\partial_z f(z, v)) \quad (2.11)$$

$$G = 2\sqrt{f_0}z \quad (2.12)$$

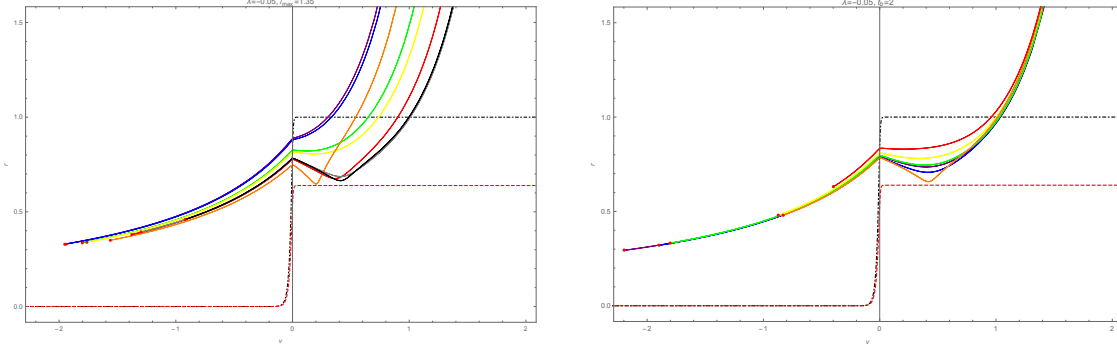


Figure 8. Left panel: r vs v profile of representative geodesics with $\lambda_{GB} = -0.05$ and fixed $\ell = 1.35$. Right panel: r vs v profile of representative geodesics with $\lambda_{GB} = -0.05$ and fixed $t_b = 2$

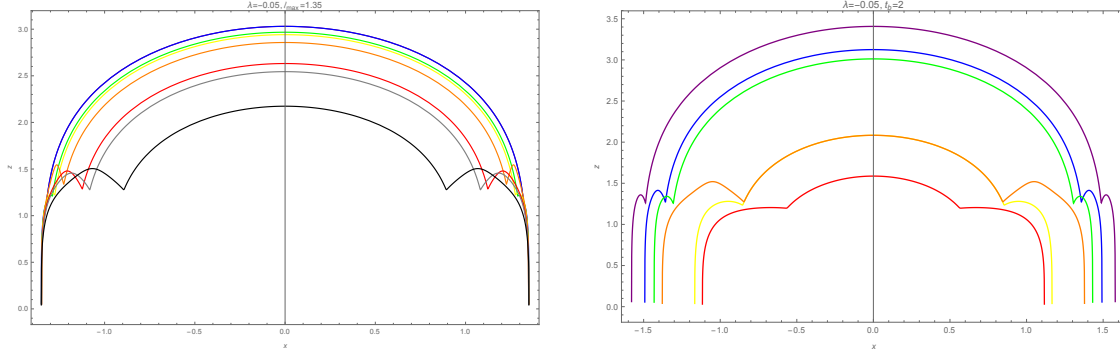


Figure 9. Left panel: x vs z profile of representative geodesics with $\lambda_{GB} = -0.05$ and fixed $\ell = 1.35$. Right panel: x vs z profile of representative geodesics with $\lambda = -0.05$ and fixed $t_b = 2$

C Minimal Volume results

In order to understand if the effects found for λ_{GB} in the entanglement entropy are due to the correction in the prescription for (4.1) or are inherent to minimal surfaces in Gauss-Bonnet we study volumes in the background (2.13). These are purely geometrical objects that are not dual to any observable in the field theory. We find, Figs.(8), (9), that for $\lambda_{GB} < 0$ there are minimal volume surfaces that, for early times, reach the singularity.

References

- [1] S. Ryu and T. Takayanagi, *Holographic derivation of entanglement entropy from AdS/CFT*, *Phys.Rev.Lett.* **96** (2006) 181602, [[hep-th/0603001](#)].

- [2] J. Abajo-Arrastia, J. Aparicio, and E. Lopez, *Holographic Evolution of Entanglement Entropy*, *JHEP* **11** (2010) 149, [[arXiv:1006.4090](#)].
- [3] V. E. Hubeny, H. Maxfield, M. Rangamani, and E. Tonni, *Holographic entanglement plateaux*, *JHEP* **1308** (2013) 092, [[arXiv:1306.4004](#)].
- [4] V. E. Hubeny and H. Maxfield, *Holographic probes of collapsing black holes*, *JHEP* **1403** (2014) 097, [[arXiv:1312.6887](#)].
- [5] H. Liu and S. J. Suh, *Entanglement growth during thermalization in holographic systems*, *Phys.Rev.* **D89** (2014), no. 6 066012, [[arXiv:1311.1200](#)].
- [6] B. Freivogel, R. A. Jefferson, L. Kabir, B. Mosk, and I.-S. Yang, *Casting Shadows on Holographic Reconstruction*, [arXiv:1412.5175](#).
- [7] V. E. Hubeny and M. Rangamani, *Causal Holographic Information*, *JHEP* **1206** (2012) 114, [[arXiv:1204.1698](#)].
- [8] V. Balasubramanian, B. D. Chowdhury, B. Czech, and J. de Boer, *Entwinement and the emergence of spacetime*, *JHEP* **1501** (2015) 048, [[arXiv:1406.5859](#)].
- [9] A. Buchel, J. Escobedo, R. C. Myers, M. F. Paulos, A. Sinha, et al., *Holographic GB gravity in arbitrary dimensions*, *JHEP* **1003** (2010) 111, [[arXiv:0911.4257](#)].
- [10] D. M. Hofman and J. Maldacena, *Conformal collider physics: Energy and charge correlations*, *JHEP* **0805** (2008) 012, [[arXiv:0803.1467](#)].
- [11] X. O. Camanho, J. D. Edelstein, J. Maldacena, and A. Zhiboedov, *Causality Constraints on Corrections to the Graviton Three-Point Coupling*, [arXiv:1407.5597](#).
- [12] Y.-Z. Li, S.-F. Wu, and G.-H. Yang, *Gauss-Bonnet correction to Holographic thermalization: two-point functions, circular Wilson loops and entanglement entropy*, *Phys.Rev.* **D88** (2013) 086006, [[arXiv:1309.3764](#)].
- [13] X. Zeng and W. Liu, *Holographic thermalization in Gauss-Bonnet gravity*, *Phys.Lett.* **B726** (2013) 481–487, [[arXiv:1305.4841](#)].
- [14] X.-X. Zeng, X.-M. Liu, and W.-B. Liu, *Holographic thermalization with a chemical potential in Gauss-Bonnet gravity*, *JHEP* **1403** (2014) 031, [[arXiv:1311.0718](#)].
- [15] V. Jahnke, A. S. Misobuchi, and D. Trancanelli, *Holographic renormalization and anisotropic black branes in higher curvature gravity*, *JHEP* **01** (2015) 122, [[arXiv:1411.5964](#)].
- [16] V. E. Hubeny, M. Rangamani, and T. Takayanagi, *A Covariant holographic entanglement entropy proposal*, *JHEP* **0707** (2007) 062, [[arXiv:0705.0016](#)].
- [17] V. Balasubramanian, A. Bernamonti, J. de Boer, N. Copland, B. Craps, et al., *Holographic Thermalization*, *Phys.Rev.* **D84** (2011) 026010, [[arXiv:1103.2683](#)].

- [18] E. Caceres and A. Kundu, *Holographic Thermalization with Chemical Potential*, *JHEP* **1209** (2012) 055, [[arXiv:1205.2354](#)].
- [19] D. Galante and M. Schvellinger, *Thermalization with a chemical potential from AdS spaces*, *JHEP* **1207** (2012) 096, [[arXiv:1205.1548](#)].
- [20] E. Caceres, A. Kundu, and D.-L. Yang, *Jet Quenching and Holographic Thermalization with a Chemical Potential*, *JHEP* **1403** (2014) 073, [[arXiv:1212.5728](#)].
- [21] L.-Y. Hung, R. C. Myers, and M. Smolkin, *On Holographic Entanglement Entropy and Higher Curvature Gravity*, *JHEP* **1104** (2011) 025, [[arXiv:1101.5813](#)].
- [22] J. de Boer, M. Kulaxizi, and A. Parnachev, *Holographic Entanglement Entropy in Lovelock Gravities*, *JHEP* **1107** (2011) 109, [[arXiv:1101.5781](#)].
- [23] X. Dong, *Holographic Entanglement Entropy for General Higher Derivative Gravity*, *JHEP* **1401** (2014) 044, [[arXiv:1310.5713](#)].
- [24] J. Camps, *Generalized entropy and higher derivative Gravity*, *JHEP* **1403** (2014) 070, [[arXiv:1310.6659](#)].
- [25] M. Headrick, V. E. Hubeny, A. Lawrence, and M. Rangamani, *Causality and holographic entanglement entropy*, *JHEP* **1412** (2014) 162, [[arXiv:1408.6300](#)].
- [26] J. Erdmenger, M. Flory, and C. Sleight, *Conditions on holographic entangling surfaces in higher curvature gravity*, *JHEP* **06** (2014) 104, [[arXiv:1401.5075](#)].
- [27] X. O. Camanho and J. D. Edelstein, *A Lovelock black hole bestiary*, *Class. Quant. Grav.* **30** (2013) 035009, [[arXiv:1103.3669](#)].
- [28] R. C. Myers and A. Singh, *Comments on Holographic Entanglement Entropy and RG Flows*, *JHEP* **1204** (2012) 122, [[arXiv:1202.2068](#)].
- [29] D. G. Boulware and S. Deser, *String Generated Gravity Models*, *Phys. Rev. Lett.* **55** (1985) 2656.
- [30] R. C. Myers and B. Robinson, *Black Holes in Quasi-topological Gravity*, *JHEP* **08** (2010) 067, [[arXiv:1003.5357](#)].
- [31] R.-G. Cai, *Gauss-Bonnet black holes in AdS spaces*, *Phys. Rev.* **D65** (2002) 084014, [[hep-th/0109133](#)].
- [32] R. Callan, J.-Y. He, and M. Headrick, *Strong subadditivity and the covariant holographic entanglement entropy formula*, *JHEP* **06** (2012) 081, [[arXiv:1204.2309](#)].
- [33] E. Caceres, A. Kundu, J. F. Pedraza, and W. Tangarife, *Strong Subadditivity, Null Energy Condition and Charged Black Holes*, *JHEP* **1401** (2014) 084, [[arXiv:1304.3398](#)].
- [34] P. Figueras, V. E. Hubeny, M. Rangamani, and S. F. Ross, *Dynamical black holes and expanding plasmas*, *JHEP* **0904** (2009) 137, [[arXiv:0902.4696](#)].

- [35] J. Dormand and P. Prince, *A family of embedded runge-kutta formulae*, *Journal of Computational and Applied Mathematics* **6** (1980), no. 1 19 – 26.
- [36] E. Hairer, G. Wanner, *DoP853*, 1994.
- [37] A. Allais and E. Tonni, *Holographic evolution of the mutual information*, *JHEP* **01** (2012) 102, [[arXiv:1110.1607](#)].
- [38] P. Fonda, L. Franti, V. Kernen, E. Keski-Vakkuri, L. Thorlacius, and E. Tonni, *Holographic thermalization with Lifshitz scaling and hyperscaling violation*, *JHEP* **08** (2014) 051, [[arXiv:1401.6088](#)].
- [39] M. Alishahiha, A. F. Astaneh, and M. R. M. Mozaffar, *Thermalization in backgrounds with hyperscaling violating factor*, *Phys. Rev.* **D90** (2014), no. 4 046004, [[arXiv:1401.2807](#)].
- [40] P. Bueno and P. F. Ramirez, *Higher-curvature corrections to holographic entanglement entropy in geometries with hyperscaling violation*, *JHEP* **12** (2014) 078, [[arXiv:1408.6380](#)].
- [41] G. Knodel and J. T. Liu, *Higher derivative corrections to Lifshitz backgrounds*, *JHEP* **10** (2013) 002, [[arXiv:1305.3279](#)].
- [42] S. Bhattacharyya and S. Minwalla, *Weak Field Black Hole Formation in Asymptotically AdS Spacetimes*, *JHEP* **09** (2009) 034, [[arXiv:0904.0464](#)].
- [43] E. Caceres, A. Kundu, J. F. Pedraza, and D.-L. Yang, *Weak Field Collapse in AdS: Introducing a Charge Density*, [arXiv:1411.1744](#).